Channel Estimation and Reconstruction in Fluid Antenna System: Oversampling is Essential

Wee Kiat New, *Member, IEEE*, Kai-Kit Wong, *Fellow, IEEE*, Hao Xu, *Member, IEEE*,
Farshad Rostami Ghadi, *Member, IEEE*, Ross Murch, *Fellow, IEEE*, and Chan-Byoung Chae, *Fellow, IEEE*

Abstract—Fluid antenna system (FAS) has recently surfaced as a promising technology for the upcoming sixth generation (6G) wireless networks. Unlike traditional antenna system (TAS) with fixed antenna location, FAS introduces a flexible component in which the radiating element can switch its position within a predefined space. This capability allows FAS to achieve additional diversity and multiplexing gains. Nevertheless, to fully reap the benefits of FAS, obtaining channel state information (CSI) over the predefined space is crucial. In this paper, we study the system with a transmitter equipped with a traditional fixed antenna and a receiver with a fluid antenna by considering an electromagnetic-compliant channel model. We address the challenges of channel estimation and reconstruction using Nyquist sampling and maximum likelihood estimation (MLE) methods. Our analysis reveals a fundamental tradeoff between the accuracy of the reconstructed channel and the number of estimated channels, indicating that half-wavelength sampling is insufficient for perfect reconstruction and that oversampling is essential to enhance accuracy. Despite its advantages, oversampling can introduce practical challenges. Consequently, we propose a suboptimal sampling distance that facilitates efficient channel reconstruction. In addition, we employ the MLE method to bound the channel estimation error by ϵ, with a specific confidence interval (CI). Our findings enable us to determine the minimum number of estimated channels and the total number of pilot symbols required for efficient channel reconstruction in a given space. Lastly, we investigate the rate performance of FAS and TAS and demonstrate that FAS with imperfect CSI can outperform TAS with perfect CSI. In contrast to existing works, we also show that there is an optimal fluid antenna size that maximizes the achievable rate when considering the energy and bandwidth overheads for full CSI acquisition.

Index Terms—6G, fluid antenna system, channel estimation, channel reconstruction, electromagnetic field, Nyquist sampling.

I. INTRODUCTION

W. K. New (a.new@ucl.ac.uk), K.-K. Wong (kai-kit.wong@ucl.ac.uk), H. Xu (hao.xu@ucl.ac.uk), and F. R. Ghadi (f.rostamighadi@ucl.ac.uk) are with the Department of Electronic and Electrical Engineering, University College London, London, WC1E 6BT, United Kingdom. K.-K. Wong is also affiliated with Yonsei Frontier Lab., Yonsei University, Seoul 03722, Korea.

R. Murch (eermurch@ust.hk) is with the Department of Electronic and Computer Engineering and Institute for Advanced Study (IAS), The Hong Kong University of Science and Technology, Clear Water Bay, Hong Kong SAR, China.

C.-B. Chae (cbchae@yonsei.ac.kr) are with the School of Integrated Technology, Yonsei University, Seoul, 03722, Korea.

Corresponding author: Kai-Kit Wong.

FLUID antenna system (FAS) represents the new paradigm of shape-and-position-flexible antenna technologies that benefit from the new forms of reconfigurable antennas such as liquid-based antennas [1], [2], reconfigurable radio-frequency (RF) pixels [3], [4] or mechanical movable antenna structures [5]. The concept of FAS was originally brought into wireless communication systems in 2020 [6] and its application to the upcoming sixth-generation (6G) was discussed in [7], [8], [9]. Unlike a traditional antenna system (TAS), where the antenna location is fixed, FAS refers to any antenna structures that can intelligently adapt their shape and position to reconfigure the gain, radiation patterns, and other radiation characteristics to enhance communication performance. Recent articles in [10], [11] have reported experimental results on FAS.

Recent efforts have treated FAS as a new degree of freedom (DoF) which is dictated by its size and the number of flexible positions (a.k.a. ports). Early attempts have been to investigate the fundamental performance limits of FAS, revealing considerable gains over TAS [12], [13], [14], [15], [16], [17]. Most recently, the diversity and multiplexing gain for the multiple-input multiple-output (MIMO) FAS setup was also understood [18]. Promising results by optimizing FAS in different setups can be found in [19], [20], [21], [22]. Furthermore, there has been great interest in combining FAS with other technologies, such as reconfigurable intelligent surfaces [23], physical layer security [24], [25], non-orthogonal multiple access [26], [27], full-duplex radios [28], and index modulation [29], [30], [31]. A more complete list of recent works is included in [32].

However, most existing studies rely on full channel state information (CSI) to fully exploit the benefits of FAS. Recent advances in CSI acquisition have greatly benefited from sophisticated signal processing methods such as array processing [33], machine learning [34], the Bayesian learning framework [35], compressive sensing [36] and etc. Exploitation of channel statistics, sparsity, and correlation has also enhanced channel estimation performance by a lot [37], [38], [39]. These techniques, nonetheless, focus on scenarios with fixed radiating element locations, thereby often limiting the number of channel estimations. In contrast, in FAS scenarios, acquiring the CSI of a predefined space (i.e., full CSI) is more challenging as it involves both channel estimation and reconstruction (either interpolation or extrapolation, or both).

To obtain the full CSI, latest research has delved into the channel estimation and reconstruction problem for FAS. For example, in [28], the authors devised a sequential linear minimum mean square error (MMSE)-based channel estimation method for large-scale fluid antenna-aided full-duplex cellular networks whereas [40] employed deep learning techniques to reconstruct the channels of the unobserved ports based on the

estimated channels from a few known ports. Besides, [41] and [42] used recurrent neural networks (RNNs) and conditional generative adversarial networks (cGANs), respectively, to tackle the channel reconstruction and port selection issues in FAS. In scenarios where the channel is sparse, [43] illustrated that low-sample-size sparse channel reconstruction techniques are effective for obtaining the full CSI. Additionally, a successive Bayesian reconstructor was introduced in [44], [45] with kernel-based sampling and regression techniques, and compressed sensing methods were utilized in [46].

Collectively, these studies indicate that traditional channel estimation schemes originally designed for TAS are inadequate for FAS, as they would incur unbearable pilot overhead due to the possibility of positioning the radiating element at near-infinitely many locations. To reduce the pilot overhead, state-of-the-art methods typically only estimate the channels at a few locations and reconstruct the FAS channel over a finite space based on these initial estimates. This can be achieved by leveraging the spatial correlation of the channels, their sparsity, or any other implicit structural characteristics. Despite considerable efforts, the minimum number of estimated channels and the minimum distance between these estimated channels required to perfectly reconstruct the FAS channel over a given space remain unknown. This challenge persists partly because existing channel models provide limited insights for more fundamental analysis, especially for the continuous FAS case (i.e., when the number of ports is infinite for a given space). Note that most literature on FAS has observed that increasing the number of estimated channels or decreasing the minimum distance between the estimated channels typically enhances the accuracy of channel reconstruction.

However, recent findings in holographic MIMO and electromagnetic information theory present a contrasting perspective. Specifically, the functional DoF represents the minimum number of samples required to reconstruct a given electromagnetic field [47]. This metric is closely tied to the transmission capacity of an electromagnetic system, as the maximum number of complex values that can be transmitted within a single electromagnetic channel is equivalent to the minimum number of required samples to reconstruct a given electromagnetic field [47], [48]. It was thus argued in [47], [48], [49], [50] that half-wavelength sampling suffices to perfectly reconstruct an arbitrary electromagnetic field with any specified precision in the far-field because the electromagnetic field is band-limited. This argument is supported by analyses in the space-wave number domain or through the Petersen-Middleton's sampling theorem, both of which are closely related to the Nyquist sampling theorem. In the near-field, however, sampling at intervals smaller than half a wavelength is considered beneficial [50].

Unlike existing studies, this paper answers two key questions: What is the minimum number of estimated channels and the minimum distance between these estimated channels needed to perfectly reconstruct the FAS channel over a given space? Furthermore, using the answers to these questions, can FAS still outperform TAS? To this end, we consider a scenario in which a transmitter equipped with a traditional antenna serves a receiver equipped with a fluid antenna over an electromagnetic-compliant channel model. Specifically, the electromagnetic-compliant channel helps us understand that the channel is band-limited when an infinite plane is considered. However, considering the properties of the antenna, such as its size and shape, reveals that the channel impinging on the receive antenna experiences spectral leakage, causing it to no longer be band-limited. Additionally, the channel is affected by receiver noise, further complicating the channel estimation and reconstruction processes. Leveraging these properties, we address the channel estimation and reconstruction problem in FAS using tractable methods such as Nyquist sampling and maximum likelihood estimation (MLE).

Through these model and methods, we show that perfect reconstruction is impossible, revealing a fundamental tradeoff between the accuracy of the reconstructed channel and the number of estimated channels. This highlights the necessity of oversampling in FAS, even in far-field propagation scenarios. Furthermore, we identify the minimum number of estimated channels and the suboptimal distance between these estimated channels necessary for efficient reconstruction of the FAS channel over a finite space. Afterwards we study the rate of FAS with the channel estimation and reconstruction problem, illustrating that FAS with imperfect channels still outperforms TAS despite the necessity to estimate the CSI over a given space. Additionally, we demonstrate that there is an optimal fluid antenna size that maximizes the achievable rate. Our key contributions are summarized as follows:

- We have developed an electromagnetic-compliant channel model for FAS for the first time, covering both one-dimensional (1D) and two-dimensional (2D) fluid antenna surfaces. This model is applicable to reconfigurable pixel-based fluid antennas in which the radiating elements are adjusted in discrete manner, as well as to movable antennas or liquid-based fluid antennas, where the number of ports approaches infinity, allowing the radiating element to be repositioned continuously. More importantly, we have considered the effects of antenna size and shape, as well as noise, on channel estimation and reconstruction.

- Utilizing the Nyquist sampling theorem, we demonstrate a fundamental tradeoff between the accuracy of the reconstructed channel and the number of estimated channels. This finding underscores the necessity of oversampling in FAS to ensure accurate channel reconstruction. Furthermore, by employing the MLE method, we illustrate that the error of the estimated channels can be bounded within a specific confidence interval (CI). Through MLE, we also prove that the error of imperfect channels can be modeled as Gaussian noise only at positions where channel estimation is performed.

- To strike a balance between the accuracy of the reconstructed channel and the number of estimated channels, we propose a suboptimal sampling distance. This strategy, combined with MLE, allows us to determine the minimum number of estimated channels needed for a given space and obtain the number of pilot symbols required to efficiently estimate and reconstruct the FAS channel.

- We present comprehensive simulation results that demonstrate the practicality and efficiency of estimating and
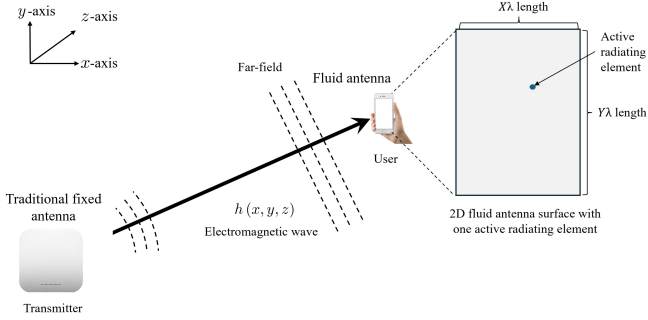
Figure 1: A point-to-point scenario with a traditional fixed antenna at the transmitter and a 2D FAS at the receiver.

reconstructing the FAS channel on both 1D and 2D fluid antenna surfaces. Additionally, our results highlight the relationships between various parameters, such as sampling distance, number of pilot symbols per sub-block, signal-to-noise ratio (SNR) and CI. More importantly, we show that FAS with imperfect CSI can outperform TAS with perfect CSI in a point-to-point scenario, and there exists an optimal fluid antenna size that maximizes the achievable rate after considering the overheads.

Note that FAS can be conceptually viewed as a holographic MIMO system with antenna selection. The reconstructed electromagnetic field can be interpreted as the reconstructed FAS channel (i.e., channels over a continuous space with infinitely many ports), while the sampling points in the electromagnetic field can be seen as the estimated channels in FAS. However, it is crucial to distinguish that an electromagnetic field is proven to be band-limited (half-wavelength sampling sufficient for perfect reconstruction) and the estimated FAS channels are affected by noise. Leveraging ports that are less than half a wavelength apart can also be interpreted as oversampling [14].

The remainder is organized as follows. Section II presents the electromagnetic-compliant channel model for FAS. In Section III, we discuss the channel estimation and reconstruction methods while deriving important parameters, relationships, tradeoffs, and rates. Simulation results are provided in Section IV. Finally, the conclusion is drawn in Section V.

II. ELECTROMAGNETIC-COMPLIANT CHANNEL MODEL

As shown in Fig. 1, this paper considers a point-to-point scenario in which a transmitter serves a receiver. We assume that the transmitter is equipped with a traditional fixed antenna, while the receiver employs a fluid antenna. Unless otherwise stated, we assume that the fluid antenna surface is 2D and has a size of $X\lambda \times Y\lambda$ where λ denotes the carrier wavelength. Furthermore, the fluid antenna has only one active radiating element. In liquid-based FAS [2], the radiating element can move to any location on the 2D fluid antenna surface. In the case of a pixel-based antenna [4], this means that certain pixels can be activated to form an active radiating element. Compared to existing works, this paper considers an electromagnetic-compliant channel model to gain better understanding into the

channel estimation and reconstruction problem.[1]

According to [51], the electromagnetic nature of small-scale fading requires that each realization channel, $h(x, y, z)$, satisfies the scalar Helmholtz equation, where (x, y, z) represents the Cartesian coordinate in a three-dimensional (3D) space. This stipulates that

$$\left(\nabla^2 + \kappa^2\right) h(x, y, z) = 0, \tag{1}$$

where (1) is a second-order linear partial differential equation with constant coefficients, ∇^2 is the Laplace operator, and $\kappa = 2\pi/\lambda$ is the wavenumber. Based on their Fourier properties, it is evident from (1) that the following condition must be met:

$$k_x^2 + k_y^2 + k_z^2 - \kappa^2 = 0. \tag{2}$$

Given k_x and k_y, we know that

$$k_z = \pm k_z(k_x, k_y) = \pm\sqrt{\kappa^2 - k_x^2 - k_y^2}. \tag{3}$$

By superposition, the general solution to (1) is given by [53]

$$h(x, y, z) = \iint_{\mathcal{D}(\kappa)} H^+(k_x, k_y) e^{j(k_x x + k_y y + k_z(k_x, k_y)z)}$$
$$+ H^-(k_x, k_y) e^{j(k_x x + k_y y - k_z(k_x, k_y)z)} dk_x dk_y, \tag{4}$$

where $H^+(k_x, k_y), H^-(k_x, k_y)$ are unknown constants and $\mathcal{D}(\kappa) = \left\{(k_x, k_y) \in \mathbb{R} \mid k_x^2 + k_y^2 \leq \kappa^2\right\}$.[2]

The spatial autocorrelation function is given as

$$c_h(x, y, z)$$
$$= \mathbb{E}\left\{h(x + x', y + y', z + z') h^*(x', y', z')\right\}. \tag{5}$$

Consequently, the power spectral density in the wavenumber domain can be derived as

$$S_h(k_x, k_y, k_z)$$
$$= \iiint c_h(x, y, z) e^{-j(k_x x + k_y y + k_z z)} dx dy dz. \tag{6}$$

Using the inverse Fourier transform, the power spectral density in the wavenumber domain can be converted back into the spatial autocorrelation function in the spatial domain by

$$c_h(x, y, z) = \frac{1}{(2\pi)^3} \iiint S_h(k_x, k_y, k_z) \times$$
$$e^{j(k_x x + k_y y + k_z z)} dk_x dk_y dk_z. \tag{7}$$

Due to (1) and the translation-invariant property, applying the Helmholtz operators to both sides of (5) results in

$$\left(\nabla^2 + \kappa^2\right) c_h(x, y, z) = 0. \tag{8}$$

---

[1]It is worth highlighting that [51], [52] are two pioneering works that established electromagnetic-compliant channel models for holographic MIMO. Motivated by these remarkable contributions, this paper adopts a similar approach to develop an electromagnetic-compliant channel model for FAS, applicable to both 1D and 2D surfaces.

[2]By assuming that $k_x^2 + k_y^2 \leq \kappa^2$, we are focusing on the far-field propagation. In the near-field, where $k_x^2 + k_y^2 > \kappa^2$, it is evident that oversampling is useful [50]. However, as we will show later in this paper, oversampling remains essential even in the far-field.

By applying the Fourier transform to both sides of (8), then we obtain

$$\left(k_x^2 + k_y^2 + k_z^2 - \kappa^2\right) S_h\left(k_x, k_y, k_z\right) = 0. \tag{9}$$

This implies that $S_h\left(k_x, k_y, k_z\right) = 0$ except at the wavenumber support, which is defined as

$$S = \left\{(k_x, k_y, k_z) \in \mathbb{R}^3 \mid k_x^2 + k_y^2 + k_z^2 = \kappa^2\right\}. \tag{10}$$

Since $k_x^2 + k_y^2 + k_z^2 = \kappa^2$ and k_z is determined by k_x and k_y, as shown in (2) and (3), respectively, we can simplify $S_h\left(k_x, k_y, k_z\right)$ as

$$S_h\left(k_x, k_y\right) = A^2\left(k_x, k_y\right) \delta\left(k_x^2 + k_y^2 + k_z^2 - \kappa^2\right), \tag{11}$$

where $A^2\left(k_x, k_y\right)$ is the non-negative real function. Using (3), we can define

$$A^2\left(k_x, k_y\right) = \begin{cases} A_+^2\left(k_x, k_y\right), & k_z\left(k_x, k_y\right) \geq 0, \\ A_-^2\left(k_x, k_y\right), & k_z\left(k_x, k_y\right) < 0, \end{cases} \quad (k_x, k_y) \in \mathcal{D}. \tag{12}$$

According to [54], the Dirac delta function can be split into the sum of two delta functions as

$$\delta\left(k_x^2 + k_y^2 + k_z^2 - \kappa^2\right) = \frac{\delta\left(k_z - k_z\left(k_x, k_y\right)\right)}{2k_z\left(k_x, k_y\right)} + \frac{\delta\left(k_y + k_z\left(k_x, k_y\right)\right)}{2k_z\left(k_x, k_y\right)}. \tag{13}$$

Substituting (12) and (13) into (11), and then taking the inverse Fourier transform with respect to (w.r.t.) k_z, we obtain

$$\frac{1}{2\pi} \int S_h\left(k_x, k_y\right) e^{j(k_z z)} dk_z \tag{14}$$

$$= \frac{A_+^2\left(k_x, k_y\right) e^{+j(k_z(k_x, k_y)z)}}{4\pi k_z\left(k_x, k_y\right)}$$

$$+ \frac{A_-^2\left(k_x, k_y\right) e^{-j(k_z(k_x, k_y)z)}}{4\pi k_z\left(k_x, k_y\right)} \tag{15}$$

$$= \iint c_h\left(x, y, z\right) e^{-j(k_x x + k_y y)} dx dy. \tag{16}$$

Note that in (15), we can define

$$S_h^\pm\left(k_x, k_y\right) = \frac{A_\pm^2\left(k_x, k_y\right)}{4\pi k_z\left(k_x, k_y\right)}, \quad (k_x, k_y) \in \mathcal{D}\left(\kappa\right), \tag{17}$$

as the plane-wave spectrum.

According to [51], the random small-scale fading effect can be modeled as

$$h\left(x, y, z\right) = \frac{1}{2\pi} \iint H\left(k_x, k_y\right)$$

$$\times e^{j(k_x x + k_y y + k_z(k_x, k_y)z)} dk_x dk_y, \tag{18}$$

$$= \frac{1}{2\pi} \iint \sum_{i=\pm} \sqrt{S_h^i\left(k_x, k_y\right)} W_i\left(k_x, k_y\right)$$

$$\times e^{j(k_x x + k_y y \pm k_z(k_x, k_y)z)} dk_x dk_y \tag{19}$$

$$= \frac{1}{2\sqrt{\pi\kappa}} \iint_{\mathcal{D}(\kappa)} \sum_{i=\pm} \frac{e^{j(k_x x + k_y y)}}{\left(\kappa^2 - k_x^2 - k_y^2\right)^{1/4}} W_i\left(k_x, k_y\right)$$

$$\times e^{\pm k_z(k_x, k_y)z} dk_x dk_y \tag{20}$$

where $H\left(k_x, k_y\right)$ is the spectrum of $h\left(x, y\right)$. Furthermore, (20) is obtained by considering a 3D isotropic channel and assuming that $h\left(x, y, z\right)$ has a unit power, which yields $A_\pm\left(k_x, k_y\right) = \frac{2\pi}{\sqrt{\kappa}}$. Also, $W_i\left(k_x, k_y\right)$ in (19) and (20) are the white Gaussian random process with unit variance, used to model the stochastic nature of the propagation.[3] With this, we can express the unknown constants as

$$H^\pm\left(k_x, k_y\right) = \begin{cases} \sqrt{S_h^i\left(k_x, k_y\right)} W_i\left(k_x, k_y\right), & (k_x, k_y) \in \mathcal{D}\left(\kappa\right), \\ 0, & \text{otherwise}. \end{cases} \tag{21}$$

If we let $z = 0$, then (20) can be rewritten as

$$h\left(x, y, 0\right) = \frac{1}{2\pi} \iint \sum_{i=\pm} \frac{\sqrt{\frac{\pi}{k}}}{\left(\kappa^2 - k_x^2 - k_y^2\right)^{1/4}} W_i\left(k_x, k_y\right)$$

$$\times e^{j(k_x x + k_y y)} dk_x dk_y. \tag{22}$$

This implies

$$S_h^\pm\left(k_x, k_y\right) = \frac{\frac{\pi}{k}}{\left(\kappa^2 - k_x^2 - k_y^2\right)^{1/2}}, \quad (k_x, k_y) \in \mathcal{D}\left(\kappa\right), \tag{23}$$

and we can further simplify (22) as

$$h\left(x, y\right) = \frac{1}{2\pi} \iint \sum_{i=\pm} \sqrt{S_h^i\left(k_x, k_y\right)} W_i\left(k_x, k_y\right)$$

$$\times e^{j(k_x x + k_y y)} dk_x dk_y. \tag{24}$$

To approximate $h\left(x, y\right)$, we divide the integration interval of (24) uniformly with frequency spacing $\Delta_{k_x} = \frac{2\pi}{L_x}$ and $\Delta_{k_y} = \frac{2\pi}{L_y}$ so that

$$h\left(x, y\right) \approx \sum_{\bar{y}=-\frac{\kappa L_y}{2\pi}}^{\frac{\kappa L_y}{2\pi}-1} \sum_{\bar{x}=-\frac{\kappa L_x}{2\pi}}^{\frac{\kappa L_x}{2\pi}-1} \sum_{i=\pm} H_{\bar{x}, \bar{y}}^i e^{j2\pi\left(\frac{\bar{x}}{L_x}x + \frac{\bar{y}}{L_y}y\right)}, \tag{25}$$

where $(\bar{x}, \bar{y}) \in \mathcal{E}$,

$$\mathcal{E} = \left\{(\bar{x}, \bar{y}) \in \mathbb{Z}^2 \left| \left(\frac{\bar{x}\lambda}{L_x}\right)^2 + \left(\frac{\bar{y}\lambda}{L_y}\right)^2 \leq 1 \right.\right\}, \tag{26}$$

and

$$H_{\bar{x}, \bar{y}}^i =$$

$$\int_{\frac{2\pi\bar{y}}{L_y}}^{\frac{2\pi(\bar{y}+1)}{L_y}} \int_{\frac{2\pi\bar{x}}{L_x}}^{\frac{2\pi(\bar{x}+1)}{L_x}} \sqrt{\frac{S_h^i\left(k_x, k_y\right)}{\left(2\pi\right)^2}} W_i\left(k_x, k_y\right) dk_x dk_y. \tag{27}$$

Here, L_x and L_y are the number of discretized intervals in k_x and k_y dimensions, while $H_{\bar{x}, \bar{y}}^i$ computes the corresponding $(\bar{x}, \bar{y})$ interval of $H^i\left(k_x, k_y\right)$.

---

[3] In (20), it is evident that the z-direction only introduces a phase difference. Therefore, no additional functional DoF is actually introduced, even if a 3D antenna surface is considered. In other words, a 3D antenna surface does not fundamentally enhance the functional DoF when the channel is electromagnetically compliant.
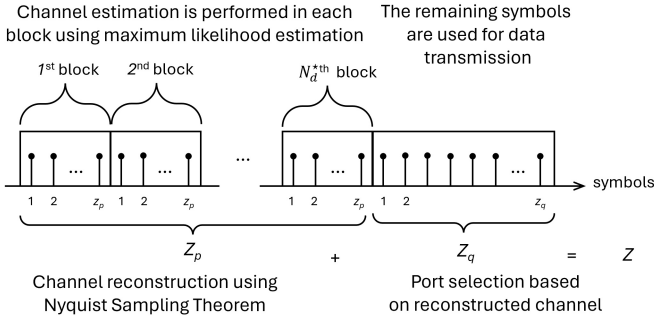
Figure 2: A schematic of the proposed channel estimation and reconstruction processes within a coherence time.

Note that $H_{\bar{x},\bar{y}}^{i}$ is a Gaussian random variable with zero mean and variance $\sigma_{i,\bar{x},\bar{y}}^{2}$. The variance $\sigma_{i,\bar{x},\bar{y}}^{2}$, can be computed as

$$\sigma_{i,\bar{x},\bar{y}}^{2} = \int_{\frac{2\pi\bar{y}}{L_y}}^{\frac{2\pi(\bar{y}+1)}{L_y}} \int_{\frac{2\pi\bar{x}}{L_x}}^{\frac{2\pi(\bar{x}+1)}{L_x}} \frac{S_h^i(k_x,k_y)}{(2\pi)^2} dk_x dk_y, \quad (28)$$

$$= \frac{1}{4\pi} \int_{\frac{\bar{y}\lambda}{L_y}}^{\frac{(\bar{y}+1)\lambda}{L_y}} \int_{\frac{\bar{x}\lambda}{L_x}}^{\frac{(\bar{x}+1)\lambda}{L_x}} \frac{\mathbf{1}_{\mathcal{D}(1)}(k_x,k_y)}{(1-k_x^2-k_y^2)^{1/2}} dk_x dk_y, \quad (29)$$

From the above derivations, it can be verified that $h(x,y)$ is band-limited because $H(k_x,k_y) \in \mathcal{D}(\kappa)$. According to the Nyquist sampling theorem [55], if $h(x,y)$ contains no frequencies higher than κ in either k_x or k_y dimensions, then $h(x,y)$ can be perfectly reconstructed by uniformly sampling the channel with $D_x, D_y \leq \frac{2\pi}{2\kappa} = \frac{\lambda}{2}$ distance. This is also known as the Nyquist sampling rate.

It is known that when a 3D isotropic channel is observed over an infinite line, the electromagnetic field is 2D. We can use similar steps to show that[4]

$$h(x) \approx \sum_{l=-\frac{\kappa L_x}{2\pi}}^{\frac{\kappa L_x}{2\pi}-1} \sum_{i=\pm} H_l^i e^{j2\pi\frac{l}{L_x}x}, \quad (30)$$

where $l \in \mathcal{E}_l$,

$$\mathcal{E}_l = \left\{ l \in \mathbb{Z} \left| \left(\frac{l\lambda}{L_x}\right)^2 \leq 1 \right. \right\}, \quad (31)$$

$$H_l^i = \int_{\frac{2\pi l}{L_x}}^{\frac{2\pi(l+1)}{L_x}} \sqrt{\frac{S_h^i(k_x)}{2\pi}} W_i(k_x) dk_x, \quad (32)$$

and its variance, $\sigma_{i,l}^2$, can be computed as

$$\sigma_{i,l}^2 = \frac{1}{\pi} \left[\arcsin\left(\frac{l+1}{L_x}\right) - \arcsin\left(\frac{l}{L_x}\right) \right]. \quad (33)$$

Similarly, $h(x)$ can be perfectly reconstructed by uniformly sampling the signal with $D_x = \frac{\lambda}{2}$ distance.

III. CHANNEL ESTIMATION AND RECONSTRUCTION USING NYQUIST SAMPLING AND MLE

As shown in Fig. 2, we consider a slow flat fading channel within a coherence time of $Z \gg 0$ digital symbols such that

[4]Note that $A_{\pm}(k_x) = 2\sqrt{\pi}$ when $h(x,y)$ has a unit power.

$Z = Z_p + Z_q$, where Z_p and Z_q are the total number of symbols used for channel estimation and data transmission, respectively. The total number of pilot symbols, Z_p, are further divided into $N_d^\star$ sub-blocks and each sub-block is dedicated to estimating the channel at a predetermined location represented by $(n_x D_x, n_y D_y)$, where $n_w \in \mathbb{Z}$ and D_w represents the sampling distance in $w \in \{x,y\}$ dimension. Each sub-block includes z_p pilot symbols for channel estimation purposes (e.g., using MLE). For brevity, we focus our analysis on the real part of the channel in this section as similar methodology can be applied to the imaginary part in parallel.

Without loss of generality, let us treat $h_{\text{FAS}}(x,y)$ as the real part of the channel of the FAS receiver at position (x,y). As it is infeasible to estimate $h_{\text{FAS}}(x,y)$ for $-\frac{X}{2}\lambda \leq x \leq \frac{X}{2}\lambda$ and $-\frac{Y}{2}\lambda \leq y \leq \frac{Y}{2}\lambda$ at every possible location, we leverage the Nyquist sampling method for channel reconstruction. Using this method, we can then determine the minimum value of $N_d^\star$ to efficiently reconstruct $\hat{h}_{\text{FAS}}(x,y)$ from $\hat{h}_{\text{FAS}}(n_x D_x, n_y D_y), \forall n_x, n_y$. Furthermore, we adopt the MLE method to estimate $\hat{h}_{\text{FAS}}(n_x D_x, n_y D_y)$. This technique ensures that the estimation error for $\hat{h}_{\text{FAS}}(n_x D_x, n_y D_y)$ remains within a bound of ε, with a specific CI. This approach ultimately enables us to determine the total number of pilot symbols required for channel estimation and reconstruction in FAS. Subsequently, we can analyze the effects of channel estimation and reconstruction on the rate of FAS.

A. 2D Nyquist Sampling Method

To reconstruct $\hat{h}_{\text{FAS}}(x,y)$, we use the 2D Nyquist sampling method. As discussed in Section II, $h(x,y)$ can be perfectly reconstructed by uniformly sampling the channel with $\frac{\lambda}{2}$ distance since $H(k_x,k_y) \in \mathcal{D}(\kappa)$. Nevertheless, a FAS receiver can only observe $h(x,y)$ over a 2D fluid antenna surface, which has a finite space of $X\lambda \times Y\lambda$. This is equivalent to multiplying $h(x,y)$ by a 2D rectangular window function

$$u(x,y) = \begin{cases} 1, & -\frac{X}{2}\lambda \leq x \leq \frac{X}{2}\lambda, -\frac{Y}{2}\lambda \leq y \leq \frac{Y}{2}\lambda, \\ 0, & \text{otherwise.} \end{cases} \quad (34)$$

As a result, the channel experienced at the FAS receiver is[5]

$$h_{\text{FAS}}(x,y) = h(x,y) u(x,y). \quad (35)$$

In the frequency domain, the spectrum of $h_{\text{FAS}}(x,y)$ can be expressed as[6]

$$H_{\text{FAS}}(k_x,k_y) = H(k_x,k_y) \circledast U(k_x,k_y), \quad (36)$$

where $\circledast$ is the 2D convolution operator. It can be easily verified that

$$U(k_x,k_y) = \frac{\sin\left(\frac{k_x}{2}X\lambda\right)}{\frac{k_x}{2}} \frac{\sin\left(\frac{k_y}{2}Y\lambda\right)}{\frac{k_y}{2}}, \quad (37)$$

[5]Compared to [51], [52], it is essential to consider the antenna properties, such as the size and shape, in FAS.

[6]Note that the terms "frequency domain" and "wavenumber domain" actually refer to the same conceptual domain. More concretely, the term "frequency domain" is commonly used in signal processing, whereas "wavenumber domain" is more frequently used in the context of physics. In this paper, we use these terms interchangeably.

where the domain of $U(k_x, k_y)$ spans over the entire $\mathbb{R}^2$.

Now, substituting (37) into (36) suggests that $H_{\text{FAS}}(k_x, k_y)$ is no longer band-limited. As a matter of fact, $U(k_x, k_y)$ leads to the spectral leakage issue. This observation aligns with the uncertainty principle [56], which states that a spatially limited signal cannot be simultaneously a band-limited signal and vice versa. This means that perfect reconstruction of $h_{\text{FAS}}(x, y)$ is impossible when the FAS receiver only observes $h(x, y)$ over a finite space of $X\lambda \times Y\lambda$. Thus, although the Nyquist sampling rate of $\frac{\lambda}{2}$ is optimal for $h(x, y)$, it is not optimal in the context of FAS, i.e., for $h_{\text{FAS}}(x, y)$. In other words, oversampling is essential in FAS to improve the accuracy of the reconstructed channel.

This raises a fundamental tradeoff between the accuracy of reconstructed channel and the number of estimated channels. Increasing the latter can introduce hardware challenges and rate degradation. For instance, a movable antenna or liquid-based fluid antenna would need to switch positions more frequently, leading to higher energy consumption, while a reconfigurable RF pixel-based fluid antenna might be subject to stronger mutual coupling. In both cases, the computational complexity of the CSI acquisition also increases. To strike a balance, we therefore propose a suboptimal method for channel reconstruction that aims to capture most of the energy of the mainlobe of $H_{\text{FAS}}(k_x, k_y)$. In particular, the spectral leakage of the mainlobe of $U(k_x, k_y)$ in the k_x- and k_y-dimensions are $\frac{2\pi}{X\lambda}$ and $\frac{2\pi}{Y\lambda}$, respectively [57]. Therefore, the spectral leakage of the mainlobe of $H_{\text{FAS}}(k_x, k_y)$ should extend to $\kappa + \frac{2\pi}{X\lambda}$ and $\kappa + \frac{2\pi}{Y\lambda}$, respectively. This means that the suboptimal sampling distance can be derived as

$$D_{x,0}^\star = \frac{2\pi}{2\left(\kappa + \frac{2\pi}{X\lambda}\right)} = \frac{\lambda}{2 + \frac{2}{X}}, \tag{38}$$

$$D_{y,0}^\star = \frac{2\pi}{2\left(\kappa + \frac{2\pi}{Y\lambda}\right)} = \frac{\lambda}{2 + \frac{2}{Y}}. \tag{39}$$

Intuitively, we can improve the channel reconstruction by further capturing the spectrum energy up to the d-th sidelobe at a cost of smaller sampling distance.[7] Since the spectral spreading of the d-th sidelobe in the k_x- and k_y-dimensions are simply $(d+1)\frac{2\pi}{X\lambda}$ and $(d+1)\frac{2\pi}{Y\lambda}$, respectively [57], the d-th suboptimal sampling distance can be expressed as

$$D_{x,d}^\star = \frac{\lambda}{2 + \frac{2}{X}(d+1)}, \tag{40}$$

$$D_{y,d}^\star = \frac{\lambda}{2 + \frac{2}{Y}(d+1)}. \tag{41}$$

Note that (38)–(41) can be regarded as the oversampling rate since it is smaller than $\frac{\lambda}{2}$ [14]. Because the size of the 2D fluid antenna surface is fixed (e.g., $X\lambda \times Y\lambda$), we can determine the number of estimated channels or sampling points for a given

[7]In practice, the propagation may not be entirely isotropic. Sampling at a smaller distance thus ensures a higher reconstruction accuracy.

space, denoted as $N_d^\star = N_{x,d}^\star N_{y,d}^\star$, where

$$N_{x,d}^\star = \left\lfloor \frac{X\lambda}{D_{x,d}^\star} \right\rfloor, \tag{42}$$

$$N_{y,d}^\star = \left\lfloor \frac{Y\lambda}{D_{y,d}^\star} \right\rfloor. \tag{43}$$

Very importantly, $N_{x,d}^\star$ and $N_{y,d}^\star$ are the minimum numbers of estimated channels that include the spectral leakage of the mainlobe or d-th sidelobe of the spectrum in the x and y dimensions, respectively.

The sampled signal can be expressed as

$$h_{\text{FAS}}^s(x, y) = \sum_{n_x \in \mathbb{Z}} \sum_{n_y \in \mathbb{Z}} \hat{h}_{\text{FAS}}\left(n_x D_{x,d}^\star, n_y D_{y,d}^\star\right) \\ \times \delta\left(x - n_x D_{x,d}^\star\right) \delta\left(y - n_y D_{y,d}^\star\right), \tag{44}$$

where $\hat{h}_{\text{FAS}}(n_x D_{x,d}^\star, n_y D_{y,d}^\star)$ represents the estimated channel at location $(n_x D_{x,d}^\star, n_y D_{y,d}^\star)$. In the frequency domain, we have

$$H_{\text{FAS}}^s(k_x, k_y) \\ = \sum_{n_x \in \mathbb{Z}} \sum_{n_y \in \mathbb{Z}} \hat{h}_{\text{FAS}}\left(n_x D_{x,d}^\star, n_y D_{y,d}^\star\right) e^{-j\left(k_x n_x D_{x,d}^\star + k_y n_y D_{y,d}^\star\right)} \\ = \frac{1}{D_{x,d}^\star D_{y,d}^\star} \sum_{l_x \in \mathbb{Z}} \sum_{l_y \in \mathbb{Z}} H_{\text{FAS}}\left(k_x - \frac{2\pi}{D_{x,d}^\star} l_x, k_y - \frac{2\pi}{D_{y,d}^\star} l_y\right). \tag{45}$$

Following the Nyquist sampling method, $\hat{h}_{\text{FAS}}(x, y)$ can be reconstructed using a low-pass filter as

$$\hat{H}_{\text{FAS}}(k_x, k_y) = H_{\text{FAS}}^s(k_x, k_y) f(k_x, k_y), \tag{46}$$

where

$$f(k_x, k_y) = \begin{cases} 1, & -\frac{2\pi}{D_{x,d}^\star} \leq k_x \leq \frac{2\pi}{D_{x,d}^\star}, -\frac{2\pi}{D_{y,d}^\star} \leq k_y \leq \frac{2\pi}{D_{y,d}^\star}, \\ 0, & \text{otherwise.} \end{cases} \tag{47}$$

Finally, we can obtain $\hat{h}_{\text{FAS}}(x, y)$ for $-\frac{X}{2}\lambda \leq x \leq \frac{X}{2}\lambda$ and $-\frac{Y}{2}\lambda \leq y \leq \frac{Y}{2}$ using the inverse Fourier transform as

$$\hat{h}_{\text{FAS}}(x, y) = \frac{1}{2\pi} \int \int \hat{H}_{\text{FAS}}(k_x, k_y) e^{-j(k_x x + k_y y)} dx dy. \tag{48}$$

The normalized mean square error (NMSE) between $\hat{h}_{\text{FAS}}(x, y)$ and $h_{\text{FAS}}(x, y)$ can be computed as

$$\text{NMSE} = \frac{\int_{-\frac{Y}{2}\lambda}^{\frac{Y}{2}\lambda} \int_{-\frac{X}{2}\lambda}^{\frac{X}{2}\lambda} \left(\hat{h}_{\text{FAS}}(x, y) - h_{\text{FAS}}(x, y)\right)^2 dx dy}{\int_{-\frac{Y}{2}\lambda}^{\frac{Y}{2}\lambda} \int_{-\frac{X}{2}\lambda}^{\frac{X}{2}\lambda} (h_{\text{FAS}}(x, y))^2 dx dy}. \tag{49}$$

The 1D counterpart can be derived in a similar fashion as will be elaborated in Appendix I.

B. MLE

For brevity, let us denote $(\boldsymbol{Dn}) = (n_x D_x, n_y D_y)$. Suppose the radiating element of the FAS receiver is located at $(\boldsymbol{Dn})$. Then the received signal at symbol z can be expressed as

$$r_z(\boldsymbol{Dn}) = h_{\text{FAS}}(\boldsymbol{Dn}) q_z + \omega_z(\boldsymbol{Dn}), \ z = 1, \ldots, z_p, \tag{50}$$

where $h_{\text{FAS}}(\boldsymbol{Dn})$ is the unknown constant channel coefficient within the coherence time, while q_z and $\omega_z(\boldsymbol{Dn})$ is, respectively, the pilot symbol and additive white Gaussian noise (AWGN) during symbol z. For simplicity, we assume that $|q_z|^2 = \frac{P}{2}$ and $\omega_z(\boldsymbol{Dn})$ is an independent Gaussian random variable with zero mean and variance of $\frac{N_0}{2}$, where P and N_0 is the transmit power and noise level, respectively.

To proceed, we can rewrite (50) as

$$\boldsymbol{r}(\boldsymbol{Dn}) = \boldsymbol{q} h_{\text{FAS}}(\boldsymbol{Dn}) + \boldsymbol{\omega}(\boldsymbol{Dn}). \qquad (51)$$

where

$$\begin{cases} \boldsymbol{r}(\boldsymbol{Dn}) = \begin{bmatrix} r_1(\boldsymbol{Dn}) & \cdots & r_{z_p}(\boldsymbol{Dn}) \end{bmatrix}^T, \\ \boldsymbol{q} = \begin{bmatrix} q_1, \ldots, q_{z_p} \end{bmatrix}^T \\ \boldsymbol{\omega}(\boldsymbol{Dn}) = \begin{bmatrix} \omega_1(\boldsymbol{Dn}), \ldots, \omega_{z_p}(\boldsymbol{Dn}) \end{bmatrix}^T. \end{cases} \qquad (52)$$

In (51), $\boldsymbol{\omega}(\boldsymbol{Dn})$ is a Gaussian random vector with zero vector mean and covariance of $\frac{N_0}{2}\boldsymbol{I}$. Hence, the joint probability density function (pdf) of $\boldsymbol{\omega}[n]$ is given by

$$f_{\boldsymbol{\omega}}(w) = \frac{1}{\pi N_0^{\frac{z_p}{2}}} \exp\left\{ -\sum_{z=1}^{z_p} \frac{(r_z(\boldsymbol{Dn}) - q_z h_{\text{FAS}}(\boldsymbol{Dn}))^2}{N_0} \right\}. \qquad (53)$$

Note that (53) can be interpreted as the likelihood function of the unknown parameter $h_{\text{FAS}}(\boldsymbol{Dn})$. Thus, the log likelihood of $h_{\text{FAS}}(\boldsymbol{Dn})$ can be found as

$$\begin{aligned} &\mathcal{L}(\boldsymbol{r}(\boldsymbol{Dn})|h_{\text{FAS}}(\boldsymbol{Dn})) \\ &= -\frac{z_p}{2} \ln(\pi N_0) - \left[\sum_{z=1}^{z_p} \frac{(r_z(\boldsymbol{Dn}) - q_z h_{\text{FAS}}(\boldsymbol{Dn}))^2}{N_0^{z_p}} \right]. \end{aligned} \qquad (54)$$

The optimal condition for maximizing (54) w.r.t. $h_{\text{FAS}}(\boldsymbol{Dn})$ (i.e., the MLE) is given by[8]

$$\begin{aligned} \hat{h}_{\text{FAS}}(\boldsymbol{Dn}) &= \frac{\boldsymbol{q}^H \boldsymbol{r}(\boldsymbol{Dn})}{\|\boldsymbol{q}\|^2}, \\ &= h_{\text{FAS}}(\boldsymbol{Dn}) + \hat{\omega}_z(\boldsymbol{Dn}), \end{aligned} \qquad (55)$$

where $\hat{\omega}_z(\boldsymbol{Dn}) = \frac{\boldsymbol{q}^H}{\|\boldsymbol{q}\|^2}\boldsymbol{\omega}(\boldsymbol{Dn})$. It can be easily verified that $\hat{h}_{\text{FAS}}(\boldsymbol{Dn})$ is also a Gaussian random variable. Specifically, it has a mean of $h_{\text{FAS}}(\boldsymbol{Dn})$ and a variance of $(z_p \text{SNR})^{-1}$. This implies that the estimator is unbiased and the average mean square error is $(z_p \text{SNR})^{-1}$. Using statistics, we can ensure that the estimation error of $\hat{h}_{\text{FAS}}(\boldsymbol{Dn})$ is less than $\varepsilon > 0$ with a CI of

$$\mathbb{P}\left\{ \left| \hat{h}_{\text{FAS}}(\boldsymbol{Dn}) - h_{\text{FAS}}(\boldsymbol{Dn}) \right| < \varepsilon \right\} = \text{erf}\left(\varepsilon \sqrt{\frac{z_p \text{SNR}}{2}} \right), \qquad (56)$$

where $\text{erf}(\cdot)$ is the error function.[9] Since the error function is an increasing function, this suggests that we can increase the

CI either by increasing ε, z_p or SNR. For some fixed ε, SNR, and γ-CI, it is worth noting that we can find the minimum value via a 1D searching method as

$$z_p^* = \left\{ \min z_p \left| \text{erf}\left(\varepsilon \sqrt{\frac{z_p \text{SNR}}{2}} \right) \geq \gamma \right. \right\}. \qquad (57)$$

Thus, the total number of pilot symbols required for channel estimation and reconstruction in FAS can be obtained as

$$Z_p = z_p N_d^\star. \qquad (58)$$

Note that if Z is not significantly larger than Z_p (e.g., fast-fading channel), adjustments can be made to parameters such as ε, SNR, and γ-CI to reduce the required symbols. Other options include employing other state-of-the-art channel estimation methods or fixing the antenna location (i.e., reducing FAS to TAS for a robust communication performance).[10]

Remark 1. In practice, the fast Fourier transform (FFT) and inverse fast Fourier transform (IFFT) are typically employed. With a frequency resolution of $F > N_d^\star$, the FFT and IFFT have a time complexity of $\mathcal{O}(F \log_2(F))$. In addition, the low-pass filter has a time complexity of $\mathcal{O}(F)$, and MLE for each location has a time-complexity of $\mathcal{O}(z_p)$. Since F and z_p are independent parameters, the overall time complexity of the proposed Nyquist sampling and MLE method is $\mathcal{O}(F \log_2(F) + N_d^\star z_p)$.

C. Data Transmission

To maximize the data rate, we assume that the radiating element of FAS is activated at the location with the maximum amplitude. In the case of perfect CSI, the optimal position is

$$(x^*, y^*) = \arg\max_{(x,y)} \left\{ |h_{\text{FAS}}(x,y)|^2 \right\}. \qquad (59)$$

The received signal is expressed as

$$r_{\text{perfect}} = h_{\text{FAS}}(x^*, y^*) q + \omega, \qquad (60)$$

where q is the random information signal and ω is the AWGN. The capacity of the FAS receiver is given as

$$R_{\text{FAS}}^* = B \log_2\left(1 + |h_{\text{FAS}}(x^*, y^*)|^2 \frac{\text{SNR}}{B} \right), \qquad (61)$$

where B is the system bandwidth and $\text{SNR} = \frac{P}{N_0}$. In the case of imperfect CSI, it is necessary to estimate the channel using the proposed Nyquist sampling and MLE methods. After that, the FAS receiver can select its port based on the estimated and reconstructed channel. The suboptimal position is

$$(x^\star, y^\star) = \arg\max_{(x,y)} \left\{ \left| \hat{h}_{\text{FAS}}(x^\star, y^\star) \right|^2 \right\}. \qquad (62)$$

With imperfect CSI, we have the received signal [58]

$$r_{\text{imperfect}} = \hat{h}_{\text{FAS}}(x^\star, y^\star) q + \omega, \qquad (63)$$

---

[8]Due to the electromagnetic properties, we assume that the distribution of $h_{\text{FAS}}(\boldsymbol{Dn})$ is not known as a priori. If the distribution of $h_{\text{FAS}}(\boldsymbol{Dn})$ is known, one can resort to the MMSE approach to further improve the channel estimation performance.

[9]It is worth noting that outside the positions where channel estimation is performed, the error depends on the reconstruction method and may not necessarily follow a Gaussian distribution.

[10]If the channel remains band-limited, the proposed method can be extended to a MIMO setup with multiple fixed-position antennas at the transmitter. The channel estimation and reconstruction for MIMO-FAS, however, remains a complicated problem and requires more detailed analysis.
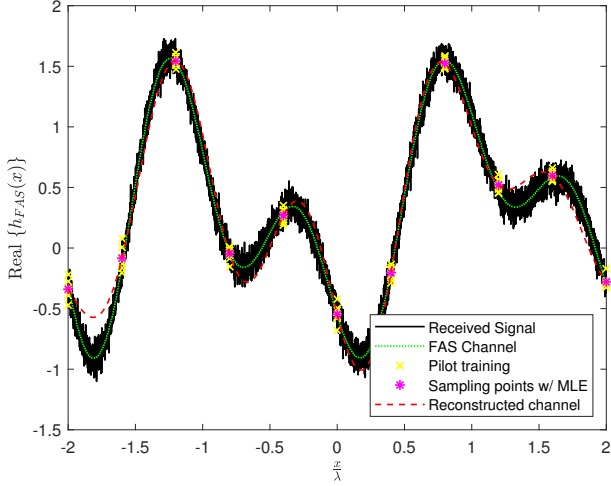
(a)
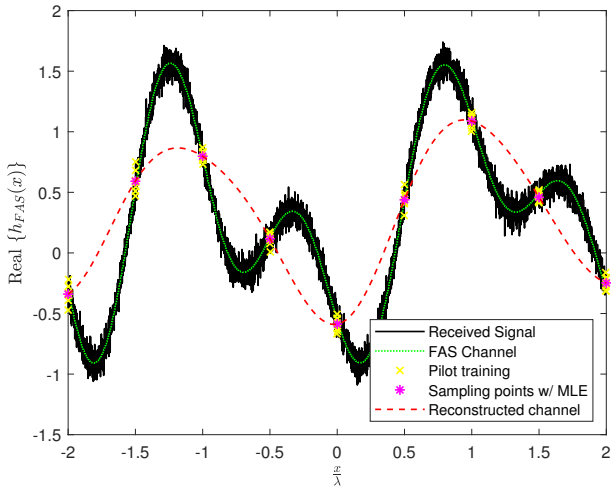
(b)

Figure 3: The fundamental effects of different parameters on a 1D channel estimation and reconstruction using: a) $D_0^\star$ sampling distance; and b) $D = \frac{\lambda}{2}$ sampling distance.

and the achievable rate can be obtained as [59]

$$R_{\text{FAS}}^\star = B \left(1 - \frac{N_d^\star z_p}{Z} \right) \log_2 \left(1 + \frac{|h_{\text{FAS}}(x^\star, y^\star)|^2 \, \text{SNR}}{|\epsilon|^2 \, \text{SNR} + B} \right), \tag{64}$$

where the additional pre-log factor accounts for the remaining symbols that can be used for data transmission per coherence time, and $\epsilon = h_{\text{FAS}}(x^\star, y^\star) - \hat{h}_{\text{FAS}}(x^\star, y^\star)$ accounts for the estimation error. Clearly, (64) shows that there is a fundamental tradeoff between high data rate and accurate channel estimation and reconstruction.

In addition, we can further consider FAS where the position of the radiating element is fixed. This is equivalent to TAS, and the capacity of TAS with perfect CSI is [58]

$$R_{\text{TAS}} = B \log_2 \left(1 + |h_{\text{FAS}}(x, y)|^2 \frac{\text{SNR}}{B} \right), \tag{65}$$

where (x, y) is an arbitrary fixed position throughout the time.
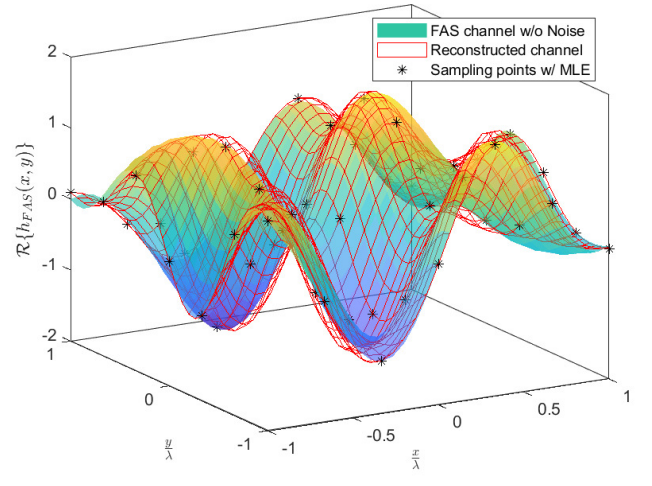
(a)
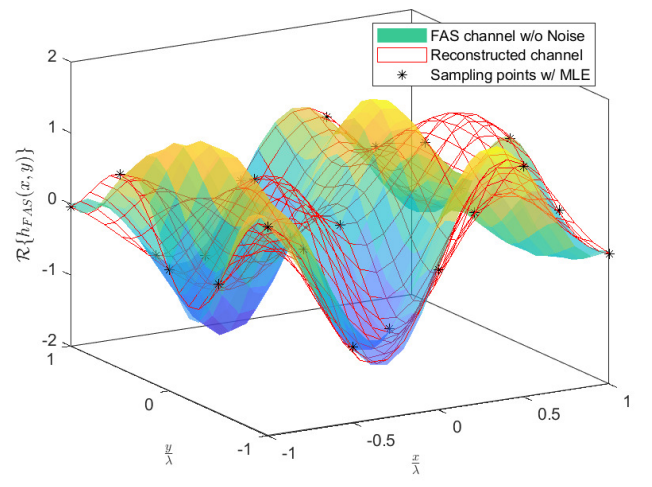
(b)

Figure 4: The 2D channel estimation and reconstruction using: a) $D_0^\star$ sampling distance; b) $D = \frac{\lambda}{2}$ sampling distance.

IV. RESULTS AND DISCUSSION

In this section, we evaluate the performance of the proposed Nyquist sampling and MLE methods for both channel estimation and reconstruction, as well as rate. For simplicity, we consider a symmetric setting; therefore, we denote W as the size and D as the sampling distance per dimension. Unless otherwise stated, we assume that $Z = 1200$, $B = 30$ KHz, $z_p = 7$, SNR = 20 dB, $L_x = L_y = 32$, $W = X = Y = 2$, and $D = D_0^\star = D_{x,0}^\star = D_{y,0}^\star$.

We first explore the fundamental effects of different parameters on the 1D channel estimation and reconstruction case, with $X = 4$. For the sake of brevity, we focus only on the real part, as similar behaviors are observed in the imaginary part. As we can see in Fig. 3, the SNR influences the variation of the received signals, while z_p determines the amount of pilot training. When the SNR is low, a higher z_p can improve the accuracy of estimated channels or sampling points by averaging out the noise effects with MLE. However,

(a)

(b)
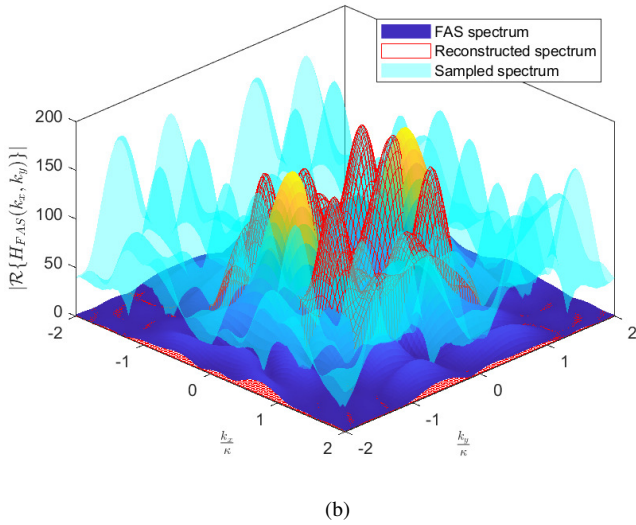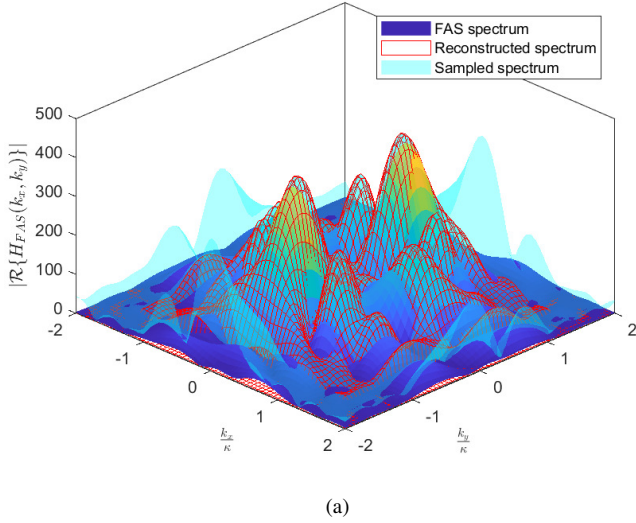
Figure 5: The 2D power spectrum density of $\hat{h}_{\mathrm{FAS}}(x,y)$ using: a) $D_0^\star$ sampling distance; b) $D = \frac{\lambda}{2}$ sampling distance.

the accuracy of the reconstructed channel strongly depends on both the accuracy of MLE at sampling points and the sampling distance. As observed in Fig. 3(b), if the sampling distance is too large, the inaccuracies in the reconstructed channel could be much more significant than those caused by the SNR, (i.e., the variation of the received signals). This suggests that the sampling distance is equally, if not more, important than the accuracy of MLE at the sampling points. Moreover, this result clearly highlights that a sampling distance of $D = \frac{\lambda}{2}$ is insufficient to perfectly reconstruct the channel.

Fig. 4 shows the 2D channel estimation and reconstruction of $h_{\mathrm{FAS}}(x,y)$ using different values of D. Similarly, we only focus on the real part as similar behaviors can be observed in the imaginary part. As it is illustrated, the FAS channel can be well estimated at each sampling point and efficiently reconstructed using the suboptimal sampling distance $D_0^\star$. This is because the effect of noise can be averaged out through the MLE, while the suboptimal sampling distance is capable of
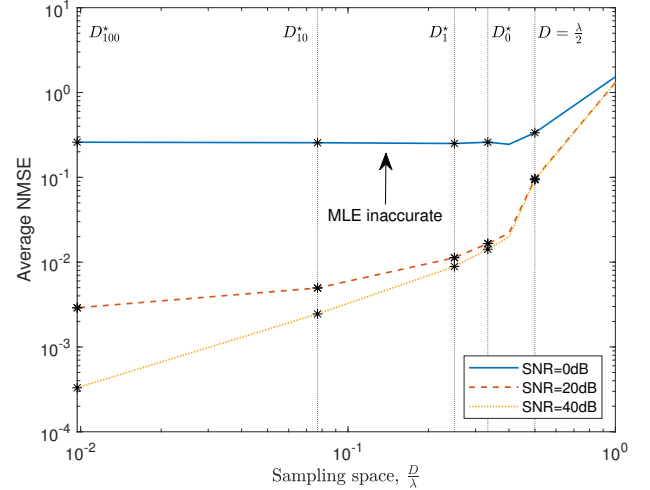
Figure 6: The tradeoff between the average NMSE and sampling distance, D.

capturing most of the energy of the spectrum. The latter can be verified by further analyzing the power spectrum density as shown in Fig. 5. When using the sampling distance $D_0^\star$, it is observed that the sampled and reconstructed spectra are able to capture the spectral leakage of the mainlobe. Nevertheless, a crucial part of spectral leakage of the mainlobe cannot be captured when using sampling distance of $D = \frac{\lambda}{2}$, leading to inaccurate channel reconstruction. For example, due to severe aliasing, we can see that $D = \frac{\lambda}{2}$ sampling distance has more compact repetition in the sampled spectrum than $D_0^\star$ sampling distance. Moreover, the reconstructed spectrum of $D = \frac{\lambda}{2}$ sampling distance does not fit well with the FAS spectrum.

Fig. 6 presents the tradeoff between the average NMSE and sampling distance, D. The sampling distance is closely related to the number of estimated channels, as revealed in (42) and (43). Since $|H_{\mathrm{FAS}}(k_x,k_y)|$ spans over the entire domain, the average NMSE generally decreases as the sampling distance decreases. However, if the MLE is inaccurate, decreasing the sampling distance may not decrease the average NMSE as shown in the low SNR case. Moreover, it is seen that if the MLE is accurate, then the decrease of the average NMSE is almost concave in a log-log scale when the sampling distance is larger than $D_0^\star$ and in contrast, the decrement of the average NMSE is approximately convex when the sampling distance is smaller than $D_0^\star$. Although smaller sampling distance decreases the average NMSE, it is worth noting that a smaller sampling distance comes with implementation complexity since it could lead to frequent position switching for liquid-based fluid antenna or strong mutual coupling for pixel-based fluid antenna. Moreover, it would also cause significant rate degradation. Thus, we suggest using the suboptimal sampling distance $D_0^\star$ as it is the largest sampling distance that at least covers the mainlobe of $|H_{\mathrm{FAS}}(k_x,k_y)|$.

Fig. 7(a) highlights the sensitivity of the sampling distance over different values of W in terms of the average NMSE. As anticipated, the average NMSE of $D = \frac{\lambda}{2}$ is evidently higher than that of $D_0^\star$ when W is small. We may think that the
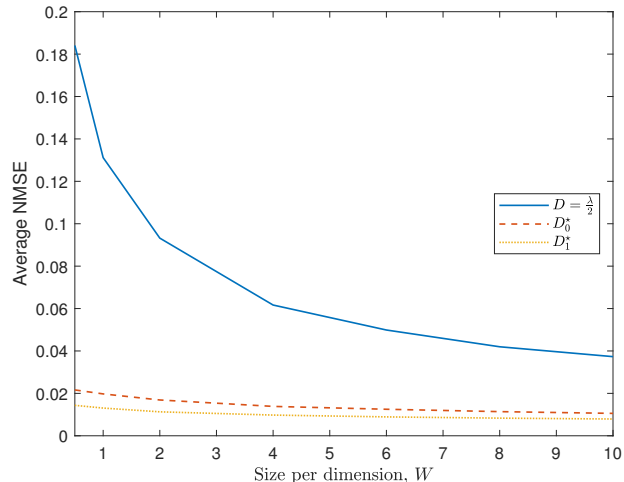
(a)
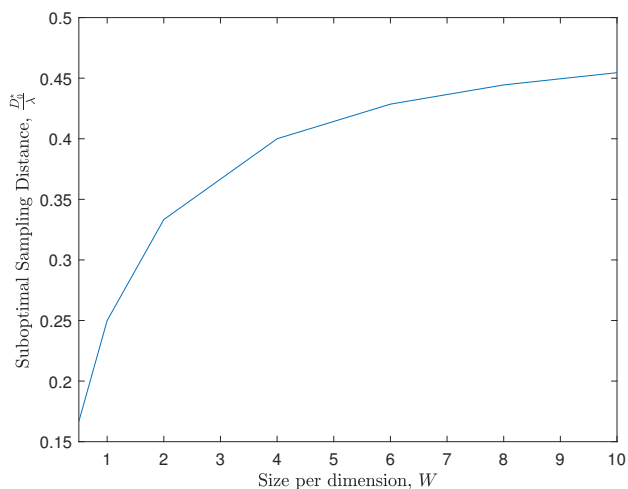
(b)

Figure 7: The sensitivity of sampling distance: a) the average NMSE versus W; b) $D_0^\star$ versus W.

average NMSE of $D = \frac{\lambda}{2}$ may converge to that of $D_0^\star$ when W is large. Nevertheless, our results show that there is still a large gap between $D_0^\star$ and $D = \frac{\lambda}{2}$ even when W is increased to 10. The reason is that $D_0^\star$ only converges to $\frac{\lambda}{2}$ at a rate proportional to $\frac{1}{W}$, as seen in Fig. 7(b). Thus, extremely large W is still required to make $\frac{\lambda}{2}$ sufficient for an efficient channel reconstruction. This suggests that a minor variation in the sampling distance can affect the average NMSE substantially when W is large. Note that when W is extremely large, the FAS receiver might be located at the near-field region. In that case, a smaller sampling distance is always useful [50].

Fig. 8 demonstrates the effects of z_p, SNR, and ε. As it is seen, the average NMSE always decreases as z_p or SNR increases. However, the effect of z_p is less substantial than the SNR. This is because in practice, z_p could only be adjusted linearly while the SNR usually ranges in the logarithmic scale. Furthermore, the numerical CI closely matches the analytical CI, and thus we can guarantee that the channel estimation error

is bounded by ε with a tractable CI, γ, implying that we can determine the value of z_p^* given some fixed ε, SNR, and γ-CI.

Fig. 9 evaluates the rates of FAS and TAS over different values of z_p. To highlight the tradeoff between high data rate and accurate channel estimation and reconstruction, we fix the SNR to 10 dB. For ease of exposition, we represent the proposed Nyquist sampling and MLE methods as FAS with imperfect CSI. As observed, FAS with perfect CSI delivers the highest data rate, followed by FAS with imperfect CSI, and finally TAS with perfect CSI. This result shows that on one hand, FAS can significantly outperform TAS while considering the channel estimation and reconstruction problem. On the other hand, there is an optimal value of z_p that maximizes the rate of FAS with imperfect CSI. Nevertheless, the optimal z_p that maximizes the achievable rate intricately depends on the system parameters D, W, Z, and SNR. Note that FAS can outperform TAS with perfect CSI because it can exploit the spatial diversity within a given space, while TAS cannot [60].

Fig. 10 compares the rate of FAS and TAS across different values of W. While existing studies suggest that increasing W is preferable for improving the FAS performance, thanks to the additional spatial diversity gain, the consideration of channel estimation alters this conclusion. Specifically, there is an optimal W that maximizes the achievable rate of FAS. This is because a larger W requires more estimated channels to efficiently reconstruct the FAS channel, which can lead to rate degradation. Therefore, a smaller W or few estimated channels may be more promising in practice.

Remark 2. *Our studies discover that the initial discrepancies stem from subtle differences in the research focus. In fields such as holographic MIMO or electromagnetic information theory, the primary concern is maximizing transmission performance. This focus often leads to the utilization of the entire continuous antenna aperture for transmission, enabling researchers to concentrate exclusively on the electromagnetic field, as the channel properties become the limiting factor for transmission efficiency. In contrast, FAS typically does not employ the entire antenna aperture for transmission. However, obtaining the full CSI is crucial to optimizing the performance of FAS. Since a FAS receiver only observes the electromagnetic field across a finite space, the received signal is not band-limited. Moreover, the channel itself might not be inherently band-limited in practice. Therefore, oversampling is essential for accurate channel reconstruction.*

V. CONCLUSION

In this paper, we investigated the problem of channel estimation and reconstruction in FAS using the Nyquist sampling and MLE methods. In contrast to prior studies, we incorporated an electromagnetic-compliant channel model to enhance our understanding in this problem. Our analysis indicated that using a half-wavelength sampling distance, though fundamental, proved inefficient in terms of NMSE due to the limited spatial reception of the FAS receiver. This spatial constraint necessitated oversampling to achieve accurate channel reconstruction, establishing a critical tradeoff between the accuracy of the reconstructed channel and the number of estimated channels.
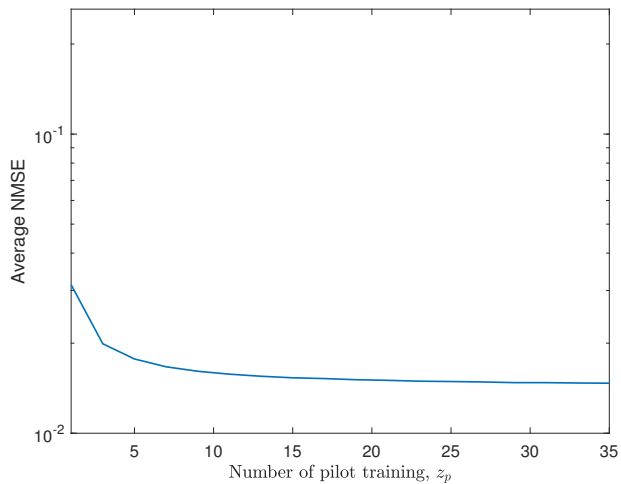
(a)
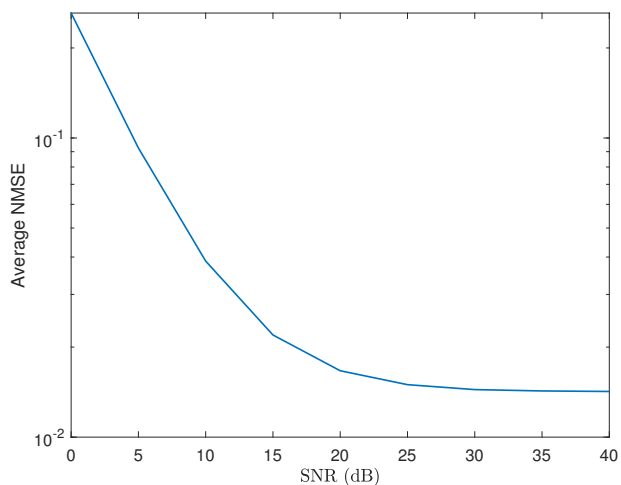
(b)
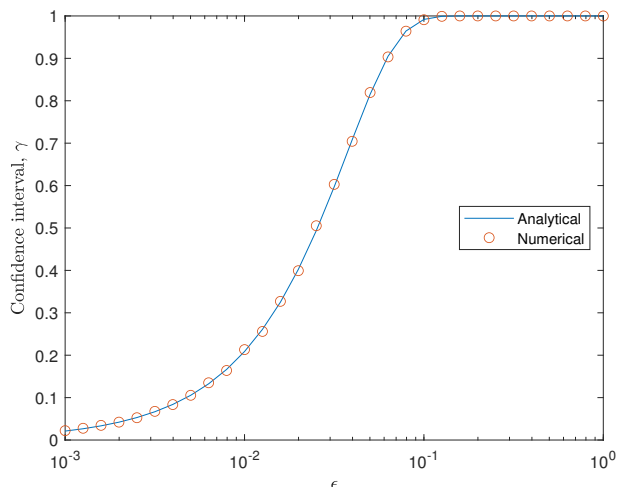
(c)

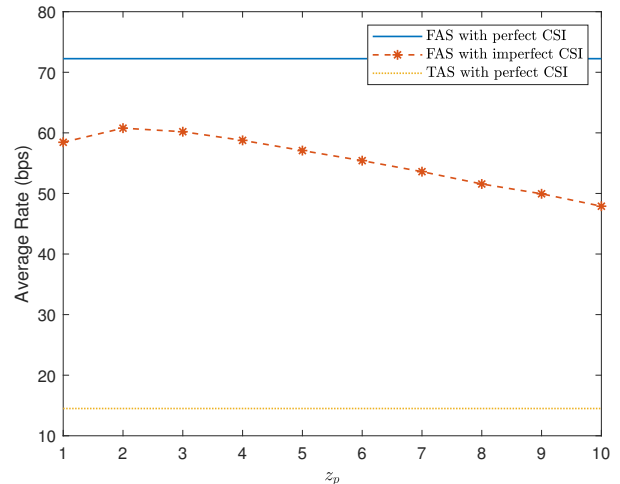Figure 8: The effects of MLE based on different values of: a) z_p; b) SNR; and c) ε.

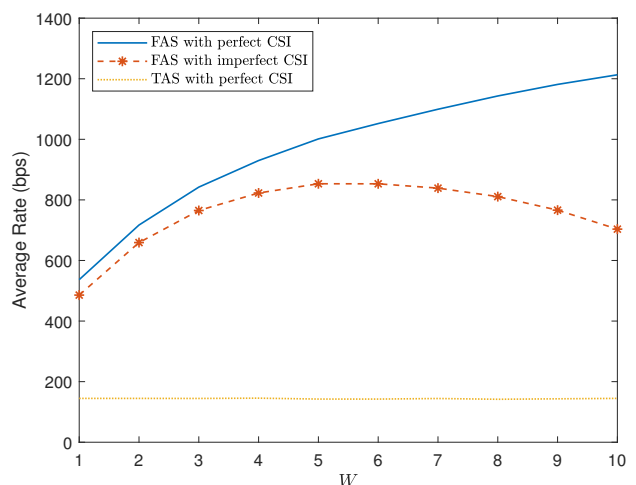Figure 9: The rates of FAS and TAS versus z_p.

Figure 10: The rates of FAS and TAS versus W.

To strike a balance between these metrics, we derived closed-form expressions for the suboptimal sampling distance and the total number of estimated channels needed for a given space. This suboptimal approach was designed to capture the majority of the energy from the mainlobe or d-th sidelobe of the channel spectrum. Additionally, we employed MLE to estimate the channel at predetermined locations, ensuring that the channel estimation error remained within a bound of ε, with a tractable CI. Our analysis further revealed the relationships between ε, z_p, SNR, and γ-CI. Utilizing these techniques allowed us to effectively determine the total number of pilot symbols required for the channel estimation and reconstruction process in FAS. Finally, we demonstrated that FAS with imperfect CSI can significantly outperform TAS with perfect CSI using the proposed Nyquist sampling and MLE methods. Furthermore, there exists an optimal W that maximizes the rate of FAS with imperfect CSI, as increasing W requires more estimated channels, potentially leading to rate degradation.

APPENDIX I: 1D NYQUIST SAMPLING METHOD

Let us denote the spatial spectrum of $h(x)$ as $H(k_x)$. In a 1D fluid antenna surface, the receiver can only observe $h(x)$ over a finite length of $X\lambda$. Thus, it is necessary to consider the following 1D rectangular window function

$$u(x) = \begin{cases} 1, & -\frac{X}{2}\lambda \leq x \leq \frac{X}{2}\lambda, \\ 0, & \text{otherwise}. \end{cases} \tag{66}$$

The channel observed at the FAS receiver is given by

$$h_{\text{FAS}}(x) = h(x)u(x). \tag{67}$$

In the frequency domain, the spectrum of $h_{\text{FAS}}(x)$ can be expressed as

$$H_{\text{FAS}}(k_x) = H(k_x) \circledast U(k_x), \tag{68}$$

where

$$U(k_x) = \frac{\sin\left(\frac{k_x}{2}X\lambda\right)}{\frac{k_x}{2}}. \tag{69}$$

Apparently, $H_{\text{FAS}}(k_x)$ is no longer band-limited. Using similar steps as the 2D Nyquist sampling method, we can obtain the d-th efficient sampling distance and the minimum number of estimated channels as

$$D_d^\star = \frac{\lambda}{2 + \frac{2}{X}(d+1)}. \tag{70}$$

and

$$N_d^\star = \left\lfloor \frac{X\lambda}{D_d^\star} \right\rfloor, \tag{71}$$

respectively.

The sampled signal in the 1D case can be expressed as

$$h_{\text{FAS}}^s(x) = \sum_{n=0}^{N_d^\star} \hat{h}_{\text{FAS}}(nD_d^\star)\delta(x - nD_d^\star). \tag{72}$$

In the frequency domain, we hence have

$$H_{\text{FAS}}^s(k) = \sum_{n=0}^{N_d^\star} \hat{h}_{\text{FAS}}(nD_d^\star)e^{-jknD_d^\star} \tag{73}$$

$$= \frac{1}{D_d^\star}\sum_{n=0}^{N_d^\star} H_{\text{FAS}}(k - nk_s^\star), \tag{74}$$

where $k_s^\star = \frac{2\pi}{D_d^\star}$ denotes the sampling frequency. Furthermore, $\hat{h}_{\text{FAS}}(x)$ can be reconstructed using a low-pass filter as

$$\hat{H}_{\text{FAS}}(k) = H_{\text{FAS}}^s(k)f(k), \tag{75}$$

where

$$f(k) = \begin{cases} 1, & -\frac{2\pi}{D_d^\star} \leq k \leq \frac{2\pi}{D_d^\star}, \\ 0, & \text{otherwise}. \end{cases} \tag{76}$$

Finally, we can obtain $\hat{h}_{\text{FAS}}(x)$ for $-\frac{X}{2}\lambda \leq x \leq \frac{X}{2}\lambda$ using the inverse Fourier transform as

$$\hat{h}_{\text{FAS}}(x) = \frac{1}{2\pi}\int \hat{H}_{\text{FAS}}(k)e^{-jk_x x}dx. \tag{77}$$

The NMSE between $\hat{h}_{\text{FAS}}(x)$ and $h_{\text{FAS}}(x)$ is simplified as

$$\text{NMSE} = \frac{\int_{-\frac{X}{2}\lambda}^{\frac{X}{2}\lambda}\left(\hat{h}_{\text{FAS}}(x) - h_{\text{FAS}}(x)\right)^2 dx}{\int_{-\frac{X}{2}\lambda}^{\frac{X}{2}\lambda}\left(h_{\text{FAS}}(x)\right)^2 dx}. \tag{78}$$

REFERENCES

[1] S. Dash, C. Psomas, and I. Krikidis, "Selection of metallic liquid in sub-6 GHz antenna design for 6G networks," *Scientific Reports*, vol. 13, no. 1, p. 20551, Nov. 2023.

[2] Y. Shen, K.-F. Tong, and K.-K. Wong, "Radiation pattern diversified single-fluid-channel surface-wave antenna for mobile communications," in *Proc. IEEE-APS Topical Conf. Antennas & Propag. Wireless Commun.*, pp. 49–51, 5-9 Sept. 2022, Cape Town, South Africa.

[3] B. Cetiner *et al.*, "Multifunctional reconfigurable MEMS integrated antennas for adaptive MIMO systems," *IEEE Commun. Mag.*, vol. 42, no. 12, pp. 62–70, Dec. 2004.

[4] L. Jing, M. Li, and R. Murch, "Compact pattern reconfigurable pixel antenna with diagonal pixel connections," *IEEE Trans. Antennas & Propag.*, vol. 70, no. 10, pp. 8951–8961, Oct. 2022.

[5] S. Basbug, "Design and synthesis of antenna array with movable elements along semicircular paths," *IEEE Antennas & Wireless Propag. Lett.*, vol. 16, pp. 3059–3062, Oct. 2017.

[6] K.-K. Wong, K.-F. Tong, Y. Zhang, and Z. Zheng, "Fluid antenna system for 6G: When Bruce Lee inspires wireless communications," *Elect. Lett.*, vol. 56, no. 24, pp. 1288–1290, Nov. 2020.

[7] K.-K. Wong, K.-F. Tong, Y. Shen, Y. Chen, and Y. Zhang, "Bruce Lee-inspired fluid antenna system: Six research topics and the potentials for 6G," *Frontiers Commun. Netw.*, vol. 3, no. 853416, Mar. 2022.

[8] A. Shojaeifard *et al.*, "MIMO evolution beyond 5G through reconfigurable intelligent surfaces and fluid antenna systems," *Proc. IEEE*, vol. 110, no. 9, pp. 1244–1265, Sept. 2022.

[9] J. Zheng *et al.*, "Flexible-position MIMO for wireless communications: Fundamentals, challenges, and future directions," *IEEE Wireless Commun.*, vol. 31, no. 5, pp. 18–26, Oct. 2024.

[10] Y. Shen *et al.*, "Design and implementation of mmWave surface wave enabled fluid antennas and experimental results for fluid antenna multiple access," *arXiv preprint*, arXiv:2405.09663, May 2024.

[11] J. Zhang *et al.*, "A novel pixel-based reconfigurable antenna applied in fluid antenna systems with high switching speed," accepted in *IEEE Open J. Antennas & Propag.*, 2024.

[12] K.-K. Wong, A. Shojaeifard, K.-F. Tong, and Y. Zhang, "Fluid antenna systems," *IEEE Trans. Wireless Commun.*, vol. 20, no. 3, pp. 1950–1962, Mar. 2021.

[13] M. Khammassi, A. Kammoun, and M.-S. Alouini, "A new analytical approximation of the fluid antenna system channel," *IEEE Trans. Wireless Commun.*, vol. 22, no. 12, pp. 8843–8858, Dec. 2023.

[14] P. Ramírez-Espinosa, D. Morales-Jimenez, and K.-K. Wong, "A new spatial block-correlation model for fluid antenna systems," *IEEE Trans. Wireless Communications*, early access, doi:10.1109/TWC.2024.3434509, Aug. 2024.

[15] W. K. New, K.-K. Wong, H. Xu, K.-F. Tong, and C.-B. Chae, "Fluid antenna system: New insights on outage probability and diversity gain," *IEEE Trans. Wireless Commun.*, vol. 23, no. 1, pp. 128–140, Jan. 2024.

[16] P. D. Alvim *et al.*, "On the performance of fluid antennas systems under α-μ fading channels," *IEEE Wireless Commun. Lett.*, vol. 13, no. 1, pp. 108–112, Jan. 2024.

[17] J. D. Vega-Sanchez, A. E. Lopez-Ramirez, L. Urquiza-Aguiar, and D. P. M. Osorio, "Novel expressions for the outage probability and diversity gains in fluid antenna system," *IEEE Wirel. Commun. Lett.*, vol. 13, no. 2, pp. 372–376, Feb. 2024

[18] W. K. New, K. K. Wong, H. Xu, K. F. Tong and C.-B. Chae, "An information-theoretic characterization of MIMO-FAS: Optimization, diversity-multiplexing tradeoff and q-outage capacity," *IEEE Trans. Wireless Commun.*, vol. 23, no. 6, pp. 5541–5556, Jun. 2024.

[19] Y. Chen, S. Li, Y. Hou, and X. Tao, "Energy-efficiency optimization for slow fluid antenna multiple access using mean-field game," *IEEE Wireless Commun. Lett.*, vol. 13, no. 4, pp. 915–918, Apr. 2024.

[20] L. Zhu, W. Ma, B. Ning, and R. Zhang, "Movable-antenna enhanced multiuser communication via antenna position optimization," *IEEE Trans. Wireless Commun.*, vol. 23, no. 7, pp. 7214–7229, Jul. 2024.

[21] H. Xu *et al.*, "Capacity maximization for FAS-assisted multiple access channels," *arXiv preprint*, arXiv:2311.11037, 2023.

[22] C. Wang *et al.*, "Fluid antenna system liberating multiuser MIMO for ISAC via deep reinforcement learning," *IEEE Trans. Wireless Commun.*, vol. 23, no. 9, pp. 10879–10894, Sept. 2024.

[23] F. R. Ghadi *et al.*, "On performance of RIS-aided fluid antenna systems," *IEEE Wireless Commun. Lett.*, vol. 13, no. 8, pp. 2175–2179, Aug. 2024.

[24] B. Tang *et al.*, "Fluid antenna enabling secret communications," *IEEE Commun. Lett.*, vol. 27, no. 6, pp. 1491–1495, Jun. 2023.

[25] J. D. Vega-Sanchez, L. Urquiza-Aguiar, H. R. C. Mora, N. V. O. Garzon and D. P. M. Osorio, "Fluid antenna system: Secrecy outage probability analysis," *IEEE Trans. Veh. Technol.*, vol. 73, no. 8, pp. 11458–11469, Aug. 2024.

[26] L. Tlebaldiyeva, S. Arzykulov, T. A. Tsiftsis, and G. Nauryzbayev, "Full-duplex cooperative NOMA-based mmWave networks with fluid antenna system (FAS) receivers," in *Proc. Inter. Balkan Conf. Commun. Netw.*, 5-8 Jun. 2023, Istanbul, Turkey.

[27] W. K. New *et al.*, "Fluid antenna system enhancing orthogonal and non-orthogonal multiple access," *IEEE Commun. Lett.*, vol. 28, no. 1, pp. 218–222, Jan. 2024.

[28] C. Skouroumounis and I. Krikidis, "Fluid antenna-aided full duplex communications: A macroscopic point-of-view," *IEEE J. Select. Areas Commun.*, vol. 41, no. 9, pp. 2879–2892, Sept. 2023.

[29] J. Zhu *et al.*, "Index modulation for fluid antenna-assisted MIMO communications: System design and performance analysis," *IEEE Trans. Wireless Commun.*, vol. 23, no. 8, pp. 9701–9713, Aug. 2024.

[30] Y. Chen, and T. Xu, "Fluid antenna index modulation communications," *IEEE Wireless Commun. Lett.*, vol. 13, no. 4, pp. 1203–1207, Apr. 2024.

[31] H. Yang *et al.*, "Position index modulation for fluid antenna system," *IEEE Trans. Wireless Commun.*, early access, doi:10.1109/TWC.2024.3446658, Aug. 2024.

[32] L. Zhu and K. K. Wong, "Historical review of fluid antenna and movable antenna," *arXiv preprint*, arXiv:2401.02362v2, 2024.

[33] M. Wang, F. Gao, S. Jin, and H. Lin, "An overview of enhanced massive MIMO with array signal processing techniques," *IEEE J. Select. Topics Sig. Process.*, vol. 13, no. 5, pp. 886–901, Sept. 2019.

[34] D. Neumann, T. Wiese, and W. Utschick, "Learning the MMSE channel estimator," *IEEE Trans. Sig. Process.*, vol. 66, no. 11, pp. 2905–2917, Jun. 2018.

[35] L. Cheng, F. Yin, S. Theodoridis, S. Chatzis, and T.-H. Chang, "Rethinking Bayesian learning for data analysis: The art of prior and inference in sparsity-aware modeling," *IEEE Sig. Process. Mag.*, vol. 39, no. 6, pp. 18–52, Nov. 2022.

[36] M. F. Duarte and Y. C. Eldar, "Structured compressed sensing: From theory to applications," *IEEE Trans. Sig. Process.*, vol. 59, no. 9, pp. 4053–4085, Sept. 2011.

[37] G. Zhou, C. Pan, H. Ren, P. Popovski, and A. L. Swindlehurst, "Channel estimation for RIS-aided multiuser millimeter-wave systems," *IEEE Trans. Sig. Process.*, vol. 70, pp. 1478–1492, Mar. 2022.

[38] G. Zhou, C. Pan, H. Ren, K. Wang, and A. Nallanathan, "A framework of robust transmission design for IRS-aided MISO communications with imperfect cascaded channels," *IEEE Trans. Sig. Process.*, vol. 68, pp. 5092–5106, Aug. 2020.

[39] Z. Peng *et al.*, "Two-stage channel estimation for RIS-aided multiuser mmWave systems with reduced error propagation and pilot overhead," *IEEE Trans. Sig. Process.*, vol. 71, pp. 3607–3622, Sept. 2023.

[40] H. Zhang *et al.*, "Learning-induced channel extrapolation for fluid antenna systems using asymmetric graph masked autoencoder," *IEEE Wireless Commun. Lett.*, vol. 13, no. 6, pp. 1665–1669, Jun. 2024.

[41] N. Waqar, K.-K. Wong, K.-F. Tong, A. Sharples, and Y. Zhang, "Deep learning enabled slow fluid antenna multiple access," *IEEE Commun. Lett.*, vol. 27, no. 3, pp. 861–865, Mar. 2023.

[42] M. Eskandari, A. Burr, K. Cumanan, and K. K. Wong, "cGAN-based slow fluid antenna multiple access," *IEEE Wireless Commun. Lett.*, vol. 13, no. 10, pp. 2907–2911, Oct. 2024.

[43] H. Xu *et al.*, "Channel estimation for FAS-assisted multiuser mmWave systems," *IEEE Commun. Lett.*, vol. 23, no. 3, pp. 632–636, Mar. 2024.

[44] Z. Zhang, J. Zhu, L. Dai, and R. W. Heath Jr, "Successive Bayesian reconstructor for channel estimation in fluid antenna systems," in Proc. *IEEE Wireless Commun. Netw. Conf.*, 21-24 Apr. 2024, Dubai, United Arab Emirates.

[45] Z. Zhang, J. Zhu, L. Dai, and R. W. Heath Jr, "Successive Bayesian reconstructor for channel estimation in fluid antenna systems," *arXiv preprint*, arXiv:2312.06551, 2023.

[46] W. Ma, L. Zhu, and R. Zhang, "Compressed sensing based channel estimation for movable antenna communications," *IEEE Commun. Lett.*, vol. 27, no. 10, pp. 2747–2751, Oct. 2023.

[47] J. Zhu, Z. Wan, L. Dai, M. Debbah, and H. V. Poor, "Electromagnetic information theory: Fundamentals, modeling, applications, and open problems," *IEEE Wireless Commun.*, vol. 31, no. 3, pp. 156–162, Mar. 2024.

[48] E. Bjornson *et al.*, "Towards 6G MIMO: Massive spatial multiplexing, dense arrays, and interplay between electromagnetics and processing," *arXiv preprint*, arXiv:2401.02844, 2024.

[49] A. Pizzo, A. d. J. Torres, L. Sanguinetti, and T. L. Marzetta, "Nyquist sampling and degrees of freedom of electromagnetic fields," *IEEE Trans. Sig. Process.*, vol. 70, pp. 3935–3947, Jun. 2022.

[50] M. Di Renzo and M. D. Migliore, "Electromagnetic signal and information theory–on electromagnetically consistent communication models for the transmission and processing of information," *arXiv preprint*, arXiv:2311.06661, 2023.

[51] T. L. Marzetta, "Spatially-stationary propagating random field model for massive MIMO small-scale fading," in Proc. *IEEE Int. Symp. Inform. Theory*, pp. 391–395, 17-22 Jun. 2018, Vail, Colorado, USA.

[52] A. Pizzo, T. L. Marzetta, and L. Sanguinetti, "Spatially-stationary model for holographic MIMO small-scale fading," *IEEE J. Select. Areas Commun.*, vol. 38, no. 9, pp. 1964–1979, Sept. 2020.

[53] F. B. Hildebrand, *Advanced calculus for applications*, Pearson, 2nd Edition, 1962.

[54] V. Balakrishnan, "All about the Dirac delta function (?)," *Resonance*, vol. 8, no. 8, pp. 48–58, 2003.

[55] C. Shannon, "Communication in the presence of noise," *Proc. IRE*, vol. 37, no. 1, pp. 10–21, 1949.

[56] H. Landau, "An overview of time and frequency limiting," *Fourier Tech. & Appl.*, pp. 201–220, 1985.

[57] B. P. Lathi and R. A. Green, *Linear systems and signals*, vol. 2, Oxford University Press New York, 2005.

[58] M. Medard, "The effect upon channel capacity in wireless communications of perfect and imperfect knowledge of the channel," *IEEE Trans. Inform. Theory*, vol. 46, no. 3, pp. 933–946, May 2000.

[59] E. Biglieri, J. Proakis, and S. Shamai, "Fading channels: Information-theoretic and communications aspects," *IEEE Trans. Inform. Theory*, vol. 44, no. 6, pp. 2619–2692, Oct. 1998.

[60] W. K. New *et al.*, "A tutorial on fluid antenna system for 6G networks: Encompassing communication theory, optimization methods and hardware designs," *arXiv preprint*, arXiv:2407.03449, Jul. 2024.

(Aven) Wee Kiat New received his Ph.D in Electrical Engineering from Universiti Teknologi Malaysia, M.Eng.Sc in Electrical Engineering from University of Malaya and B.IT in Data Communications and Networking from Multimedia University. He was a visiting researcher at Lancaster University and University of Cyprus. He is currently a research fellow at the Department of Electronic and Electrical Engineering, University College London, UK. His research interests are information theory, optimization, stochastic processes, machine learning and their applications in emerging areas of communications. He was the recipient of the 2021 IEEE Malaysia Comsoc/VTS best paper award, 2021 and 2020 IEEE Malaysia AP/MTT/EMC best paper awards.

(Kit) Kai-Kit Wong (M'01-SM'08-F'16) was born in Hong Kong in 1973. He received the BEng, the MPhil, and the PhD degrees, all in Electrical and Electronic Engineering, from the Hong Kong University of Science and Technology, Hong Kong, in 1996, 1998, and 2001, respectively. After graduation, he took up academic and research positions at the University of Hong Kong, Hong Kong, Lucent Technologies, Bell-Labs, Holmdel, the Smart Antennas Research Group of Stanford University, USA, and the University of Hull, U.K. Presently he is Chair Professor of Wireless Communications at the Department of Electronic and Electrical Engineering, University College London, U.K. He is Fellow of IEEE and IET. He served as the Editor-in-Chief for IEEE Wireless Communications Letters between 2020 and 2023. He is currently the Subject Editor-in-Chief for Wireless Communications for IET Electronics Letters and also on the Advisory Board of IEEE Communications Letters and the Steering Committee of IEEE Wireless Communications Letters.